Applied Nanoscience (2018) 8:475–488
https://doi.org/10.1007/s13204-018-0669-0

ORIGINAL ARTICLE

Highly catalytic activity of nickel nanoparticles generated in poly(methylmethacrylate)@poly(2-hydroxyethylmethacrylate) (PMMA@PHEMA) core–shell micelles for the reduction of 4-nitrophenol (4-NP)

Patharawadee Boonying[1] · **Surangkhana Martwiset**[1,2] · **Sittipong Amnuaypanich**[1,2]

Received: 27 October 2017 / Accepted: 30 January 2018 / Published online: 24 February 2018

Abstract
Excellent catalytic reduction of 4-NP in aqueous solution was achieved under ambient condition using nickel (Ni) nanoparticles generated in PMMA@PHEMA polymeric micelles. Ni nanoparticles were formed in two different PMMA@PHEMA micelles, namely Ni-loaded $PMMA_{10K}$@$PHEMA_{5K}$ and Ni-loaded $PMMA_{12K}$@$PHEMA_{34K}$ which resulted in the distinctive differences in Ni content as well as the sizes of Ni nanoparticles. Besides the concentration of the catalyst, the reduction rate of 4-NP depended on PMMA@PHEMA micelle structure, i.e., higher catalytic activity was observed for Ni-loaded $PMMA_{10K}$@$PHEMA_{5K}$. More importantly, the catalytic performance of Ni-loaded $PMMA_{12K}$@$PHEMA_{34K}$ was markedly improved with increasing amount of PHEMA-shell crosslinker despite a reduction of Ni content in the micelles.

Keywords Catalytic reduction · 4-Nitrophenol · Nickel · Micelles · Nanoparticles

Introduction

Metal nanoparticles (Metal NPs) have gained tremendous interest in the heterogeneous catalysis due to the superior catalytic properties over their bulks. A large surface-to-volume ratio of metal NPs brings high activity and high selectivity to the catalysis (Astruc 2008). Among the catalysts developed from the transition metals NPs, noble metal NPs have been utilized extensively because they possess a high chemical stability in addition to an excellent catalytic activity (Cuenya 2013). Nevertheless, these remarkable catalytic properties of noble metal NPs come with a high price because of their low earth abundance. Many attentions, therefore, have moved toward non-precious transition metals, particularly nickel nanoparticles (Ni NPs) for the catalysis applications.

Nickel is low-cost metal which is efficiently used as the catalyst for the organic synthesis. Some of the advantages of nickel catalysts include high performance in reactions compared with other metals and transformations involving unreactive substrates, facile activation and transformation of chemically less reactive molecules and large variability of electronic states (Ananikov 2015). For the Ni NPs, they are catalytically active for the hydrogenation and the transfer hydrogenation whose benefits have been found in the petrochemical and food industries (Fan et al. 2016; Panwar et al. 2015; Mortensen et al. 2016; Jiang et al. 2015; Vijayakrishna et al. 2016). Potentially, Ni NPs would be utilized as the catalyst for the water treatment (Tang et al. 2014; Demirci and Sahiner 2015). One of obvious examples is a transform of highly toxic 4-NP to less harmful 4-aminophenol (4-AP) by the catalytic reduction (Aditya et al. 2015). 4-NP is used as raw materials or intermediates in many chemical industrials (Xu et al. 2015; Zhao et al. 2010), however, due to its toxicity; it is listed as one of the priority pollutants by

Electronic supplementary material The online version of this article (https://doi.org/10.1007/s13204-018-0669-0) contains supplementary material, which is available to authorized users.

✉ Sittipong Amnuaypanich
asitti@kku.ac.th

[1] Applied Chemistry Division, Department of Chemistry and Center of Excellence for Innovation in Chemistry (PERCH-CIC), Faculty of Science, Khon Kaen University, Khon Kaen 40002, Thailand

[2] Materials Chemistry Research Center (MCRC-KKU), Faculty of Science, Khon Kaen University, Khon Kaen 40002, Thailand

U.S. Environmental Protection Agency (U.S. EPA) (Priority Pollutant List 2014) and thus requires the treatment prior to a discharge. In treating 4-NP contaminated water, the reduction of 4-NP to 4-AP by the catalytic reduction offers some advantages according to the facts that: (1) 4-AP is less toxic and is an important intermediate for the pharmaceutical industry including the manufactures of paracetamol, analgesic and antipyretic drugs (Kang et al. 2005; Dionigi et al. 2014; Zhang and Wu 2010), (2) the reduction of 4-NP to 4-AP can proceed in aqueous phase under ambient conditions (Gangula et al. 2011; Baruah et al. 2013; Farooqi et al. 2014; Youzhi et al. 2016; Karakas et al. 2017; Xia et al. 2016) and (3) 4-NP is converted only to 4-AP within a short reaction time and without any side reaction.

The key parameters towards high catalysis performance of metal NPs in liquid medium are not only the chemoselectivity and high activity for a given reaction but also a sufficient colloidal stability during a progress of the reaction (Zahmakıran and Özkar 2011). Metal NPs with low colloidal stability are susceptible to a formation of aggregates leading to a decline in the catalytic-active surface and consequently a loss of the catalytic activity. To acquire high colloidal stability, metal NPs are normally stabilized by addition of appropriate stabilizers during their formation, particularly via the route of metal-ion reduction. Block copolymers (BCPs) have been proven to be a suitable stabilizer (Alexandridis and Tsianou 2011). In particular, the amphiphilic diblock copolymers (di-BCPs), apart from being a good stabilizer, can serve as the nanoreactors to produce well-defined metal NPs, e.g., uniform and narrow particle size distribution. Since di-BCPs consist of two blocks having dissimilar solubility in particular solvent, they can form the core–shell polymeric micelles via the self-assembly process. The core offers a locus for a reduction of metal ions to metal NPs while the shell stabilizes growing particles by inhibiting particle coalescence as well as promotes the colloidal stability of full-grown metal NPs (Antonietti et al. 1996). In addition, the use of amphiphilic BCPs allows a synthesis of metal NPs in aqueous solution which is an environmentally benign system.

Synthesis of metal NPs assisted by BCPs provides a better control of particle size and shape through as-formed BCP micelles. However, it is crucial to maintain the stability of polymeric micelle throughout the particle formation process. The formation of polymeric micelles is a dynamic process which is frequently accompanied by an exchange of polymer chains between the micelles or the fission and fusion among the micelles (Nicolai et al. 2010). Therefore, a higher stability of the polymeric micelles is gained under a suppression of these intermicellar events in which it is accomplished via either the core or the shell crosslinkings (Rodríguez-Hernández et al. 2005). Herein, PMMA-*b*-PHEMA amphiphilic BCP was introduced in the synthesis of Ni NPs. PMMA@PHEMA core–shell micelles were formed with enhanced stability by a crosslinking of PHEMA-shell using diethylenetriamine (DETA). Ni NPs were subsequently generated in PMMA@PHEMA micelles to obtain Ni-loaded PMMA@PHEMA micelles which were utilized as the catalyst for the reduction of 4-NP to 4-AP under ambient conditions. Effects of PHEMA block length and DETA shell crosslinker were studied due to the fact that both influence extensively the catalytic activity of Ni NPs. Addition of DETA shell crosslinker, in one hand, provides prolonged stability to PMMA@PHEMA micelles and, on the other hand, enhances the adsorption of the reactant resulting in a promotion of the catalytic activity.

Experimental

Materials

All chemicals for synthesizing PMMA-*b*-PHEMA copolymers were purchased from Sigma-Aldrich (St.Louis, USA) including methylmethacrylate monomer (MMA, 99%) and 2-hydroxyethyl methacrylate monomer (HEMA, 97%), *p*-Toluenesulfonyl chloride (*p*-TsCl, ≥ 98%) as the initiator, the catalyst consisting of copper (II) chloride ($CuCl_2$, 99%) and *N,N,N′,N″,N″*-pentamethyldiethylenetriamine (PMDETA, 99%) and tin (II) 2-ethylhexanoate ($Sn(EH)_2$, ~ 95%) as the reducing agent. Ethylenediamine (EDA, ≥99%) and diethylenetriamine (DETA, 99%) were also supplied from Sigma-Aldrich. Nickel(II) nitrate hexahydrate ($Ni(NO_3)_2.6H_2O$, 99%) was obtained from BDH. 4-nirophenol (4-NP) and sodium borohydride ($NaBH_4$) were supplied from Sigma-Aldrich. The monomers were cleaned by passing through a basic alumina column. Water used in the experiments was distilled and deionized (DI). Other chemicals were used as received.

Synthesis of PMMA-*b*-PHEMA by ARGET ATRP

Atom transfer radical polymerization with activators regenerated by electron transfer (ARGET ATRP) was employed in the synthesis of PMMA-Cl macroinitiator and PMMA-*b*-PHEMA copolymers. To synthesize PMMA-Cl, Cu/PMDETA complex catalyst was prepared by dissolving $CuCl_2$ (0.05 mmol) and PMDETA (0.1 mmol) in 3/2 v/v of methyl ethyl ketone (MEK) and methanol (MeOH). The complex solution was charged into a round-bottom flask and purged with nitrogen for 15 min. Next MMA (50 mmol) was added into the complex solution prior to adding *p*-TsCl (1.0 mmol) and $Sn(EH)_2$ (0.2 mmol) to initiate the polymerization. Then, the polymerization was allowed to proceed at 60 °C for 6 h. The polymerization was terminated by exposing the reaction mixture to air. The catalyst was

removed by passing the reaction mixture through an aluminum oxide column. PMMA-Cl was then obtained by precipitating in cold methanol. Precipitated PMMA-Cl was dried in a vacuum oven at 25 °C for 24 h. Subsequently, PMMA-*b*-PHEMA copolymer was synthesized by the chain extension of PMMA-Cl with HEMA monomer using also ARGET ATRP. PMMA-Cl macroinitiator (0.05 mmol), $CuCl_2$ (0.05 mmol) and PMDETA (0.1 mmol) were dissolved in 3/2 v/v of MEK/MeOH prior to charging into a round-bottom flask and purging with nitrogen for 15 min. Next $Sn(EH)_2$ (0.2 mmol) in toluene and HEMA (0.5 mmol) in ethanol were added dropwise into the mixture. The reaction mixture was then heated to 60 °C to initiate the polymerization and maintained at this temperature under nitrogen atmosphere for 16 h. After that, the mixture was exposed to air to terminate the reaction. The complex catalyst was removed by passing through aluminum oxide column and PMMA-*b*-PHEMA copolymer was precipitated out of the mixture in cold diethyl ether. The precipitated product was dried in a vacuum oven at 25 °C for 24 h.

Formation of PMMA@PHEMA micelles and synthesis of Ni-loaded PMMA@PHEMA micelles

PMMA@PHEMA core–shell polymeric micelles were formed by the solvent exchange method. Initially, PMMA-*b*-PHEMA was dissolved in common solvent, dimethylsulfoxide (99.98% DMSO, Fisher Scientific), to a concentration of 1.0 wt%. The solution was filled into a dialysis tube (Spectra/Por® 6 dialysis tube with 10,000 MWCO) which then was immersed in ethanol, the selective solvent for PHEMA block, for exchanging the solvent at 30 °C. As a consequence, PMMA-*b*-PHEMA gradually transformed to PMMA@PHEMA core–shell polymeric micelles via the self-assembly process. After 12 h of the solvent exchange, the micelle solution was removed from the dialysis tube and was filtered through 0.45 μm nylon filter. In a formation of PMMA@PHEMA core-crosslinked-shell micelles, DETA was dissolved in PMMA-*b*-PHEMA solution prior to the solvent exchange process. Critical micelle concentration (CMC) of PMMA-*b*-PHEMA in ethanol was determined in the absence and presence of DETA shell crosslinker to ascertain the concentration at an onset of PMMA@PHEMA micelle formation. PMMA-*b*-PHEMA solutions were prepared at different concentrations prior to addition of 1.0 mM Pyrene (98%, Sigma-Aldrich) in ethanol to each solution. Next, their UV absorbances were monitored at $\lambda = 334$ nm using Agilent 8453 UV–Vis spectrophotometer.

To synthesize Ni-loaded PMMA@PHEMA micelles, PMMA-*b*-PHEMA solution in DMSO was filled into a dialysis tube and then immersed in 150 mL of nickel(II) tris(ethylenediamine) complex solution in ethanol (2.75×10^{-3} mM) at 30 °C for 24 h. PMMA-*b*-PHEMA was self-assembling to PMMA@PHEMA micelles, while Ni(II) complex was encapsulated in the micelles due to its lower solubility in ethanol. Next, Ni(II) complex-loaded PMMA@PHEMA micelles were stabilized by crosslinking of PHEMA shell with DETA followed by a reduction of Ni(II) to Ni(0) using $NaBH_4$ (0.1 mM) solution for 24 h at 30 °C. As-synthesized Ni-loaded PMMA@PHEMA micelles were filtered through 0.45 μm nylon filter. Ni-loaded PMMA@PHEMA micelles were prepared under different core–shell structures corresponding to a relative molecular weight of PMMA to PHEMA. Therefore, those were designated as Ni-loaded $PMMA_{10K}$@$PHEMA_{5K}$ and Ni-loaded $PMMA_{12K}$@$PHEMA_{34K}$ where the subscripts refer to the molecular weight of each block.

Catalytic reduction of 4-NP by Ni-loaded PMMA@PHEMA

Catalytic activity of Ni-loaded PMMA@PHEMA was investigated via the reduction of 4-NP to 4-AP in the presence of $NaBH_4$. Initially, 1 mL of 4-NP aqueous solution was mixed with large excess amount of $NaBH_4$ solution, typically 50 times more concentrated. Then, 1 mL of Ni-loaded PMMA@PHEMA was added and the progress of 4-NP reduction was monitored using UV–Vis spectroscopy (Agilent Technologies).

The reusability of the catalyst was investigated by performing a series of catalytic reduction of 4-NP for five cycles. On each cycle, the UV-peak intensity of 4-NP was monitored till there was no change in the intensity, then the next cycle was started by adding the fresh solution of 4-NP into the mixture of Ni-loaded PMMA@PHEMA and $NaBH_4$.

Characterization

Molecular weights and molecular weight distributions of PMMA-Cl macroinitiator and PMMA-*b*-PHEMA block copolymers were determined by gel permeation chromatography (GPC) using LC20A (Shimadzu Corp., Japan) equipped with Waters Styragel columns (HR4) and a refractive index detector (RID10A). GPC column was operated at 80°C using 0.05 M lithium bromide (99%, Riedel de Haën) in dimethylformamide (DMF) as the eluent under a flow rate of 1.0 mL min^{-1}. ^1H-NMR analysis was performed on Varian NMR-400 MHz spectrometer (Agilent Technologies) using deuterated dimethyl sulfoxide (DMSO-d_6, 99.9%) as the solvent.

Sizes and size distributions of PMMA@PHEMA micelles and Ni-loaded PMMA@PHEMA were measured by dynamic light scattering (DLS) using Brookhaven with BI-200SM goniometer and Bi-9000 particle sizing software. DLS measurement was performed at a scattering

angle of 90° under ambient temperature. Averaged particle size along with the size distribution of each sample was obtained from the measurement for 10 times.

The morphology of PMMA@PHEMA micelles and Ni-loaded PMMA@PHEMA was observed through transmission electron microscopy (TEM) using Tecnai G^2 20 (FEI, USA). If not stated otherwise, the samples for TEM observation were stained by Osmium Tetroxide (99.8%, Sigma-Aldrich). An average diameter of the particles was obtained from measuring the particle diameter in TEM images for at least 200 particles using Image*J* software.

Amount of nickel incorporated within PMMA@PHEMA micelles was determined by inductively coupled plasma-optical emission spectrometer (ICP-OES, Perkin-Elmer Optima 2100 DV).

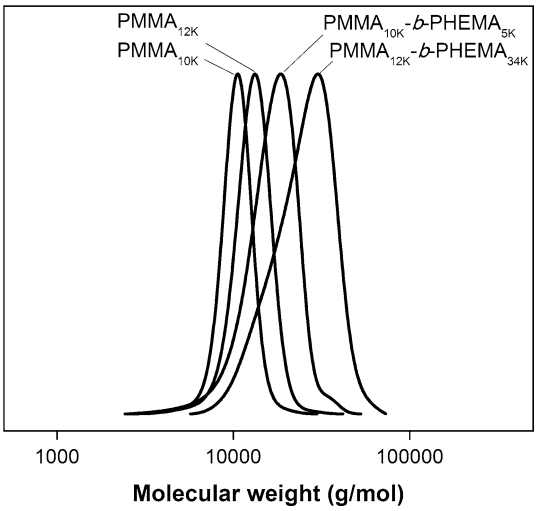

Fig. 1 Molecular weight distributions obtained from GPC of PMMA-Cl macroinitiators and PMMA-*b*-PHEMA block copolymers

Results and discussion

Synthesis of PMMA-*b*-PHEMA

Synthetic route to PMMA-*b*-PHEMA block copolymers by ARGET ATRP consists of the synthesis of PMMA-Cl macroiniator and subsequently the chain extension of PMMA-Cl with HEMA (Scheme 1 in supporting information). Figure 1 presents molecular weight distributions of PMMA-Cl and PMMA-*b*-PHEMA copolymers measured from GPC and Table 1 summarizes their corresponding number-averaged molecular weight (M_n) and polydispersity index ($Đ$). It is evidenced that PMMA-*b*-PHEMA synthesized by ARGET ATRP possessed M_n with fairly low $Đ$. In addition, M_ns of PMMA-*b*-PHEMA were well agreed with the theoretical M_n ($M_{n,th}$) assuring the characteristics of controlled/living radical polymerization (CRP).

Chemical compositions of PMMA-Cl macroinitiator and PMMA-*b*-PHEMA were confirmed by ^1H NMR as shown in Fig. S1 in supporting information. For PMMA-Cl, characteristic resonance signals appeared in the range of δ 0.77–0.94 ppm corresponding to protons of methyl group whereas methylene protons of PMMA backbone showed a broad signal around δ 1.57–2.04 ppm. Also the strong singlet methyl ester group was observed at δ 3.57 ppm. For PMMA-*b*-PHEMA, the characteristic resonance signals of PHEMA segment were at δ 4.81 ppm and δ 3.89 ppm attributing to hydroxy group (–OH) and methylene protons ($–CH_2–OH$), respectively. However, the signal intensity of methyl ester group of PMMA segment at δ 3.57 ppm was overlapped with $–O–CH_2–$ of PHEMA segment. A block composition (f_{PMMA}:f_{PHEMA}) of PMMA-*b*-PHEMA (see Table 1) was calculated from the integrals of peaks relating to peak areas of PMMA and PHEMA as described in supporting information. The mole ratio of PMMA to PHEMA block was in good agreement with that obtained from GPC.

Table 1 Number-averaged molecular weight (M_n), polydisperity index ($Đ$) and copolymer composition of PMMA-Cl macroinitiator and PMMA-*b*-PHEMA block copolymers

Block copolymers	PMMA-Cl		PMMA-*b*-PHEMA			Composition (mol %) f_{PMMA}:f_{PHEMA}	
	$M_{n,GPC}$ (g mol^{-1})	$Đ$	$M_{n,GPC}$ (g mol^{-1})	$Đ$	$M^a_{n,th}$ (g mol^{-1})	GPC	^1H NMR
$PMMA_{10K}$-*b*-$PHEMA_{5K}$	9200	1.06	15,400	1.13	17,600	60:40	58:42
$PMMA_{12K}$-*b*-$PHEMA_{34K}$	12600	1.19	47,000	1.63	35,400	27:73	26:74

[a] $M_{n,th}$ was calculated from $M_m \times$ conversion $\times [M]/[I] + M_i$, where M_m and M_i are the molar masses of the monomer and initiator and $[M]$ and $[I]$ are the concentrations of the monomer and initiator, respectively

PMMA@PHEMA micelles and Ni-loaded PMMA@PHEMA

Critical micelle concentrations (CMC) of PMMA-*b*-PHEMA were determined in ethanol in the presence and the absence of DETA. As revealed in Fig. S2 in supporting information, the plots of UV absorbance with respect to PMMA-*b*-PHEMA concentrations show distinct turns at particular concentrations of PMMA-*b*-PHEMA solutions indicating the concentration at the onset of micelle formation. CMCs, therefore, were determined as summarized in Table S1 in supporting information. CMC of PMMA-*b*-PHEMA without DETA substantially decreased with greater MW of PHEMA block. Although PHEMA is highly soluble in ethanol and one can expect higher CMC for a longer length of PHEMA block in PMMA-*b*-PHEMA, a long enough PHEMA block length gives rise to more attractions among PHEMA block and leads to a structural change from stretched segments to coil-like structures. As a result, PMMA-*b*-PHEMA becomes less soluble which eventually lowers the CMC (Astafieva et al. 1995). Upon an addition of DETA, the formation of PMMA@PHEMA micelles was promoted as evidenced by decreases in CMC for both PMMA-*b*-PHEMA. Furthermore, influence of PHEMA block length on CMC was mitigated because amino groups of DETA can impart hydrogen bonding with hydroxyl groups of PHEMA and form the crosslink structure of PHEMA-shell in PMMA@PHEMA micelles. The schematic picture of PMMA@PHEMA micelle formation is illustrated in Fig. 2. The shell crosslinking also improves the stability of the polymeric micelles by preventing the intermicellar chain exchange, thus obtaining what is so-called "frozen micelles" (Rodríguez-Hernández et al. 2005). This effect of DETA is evidenced in Fig. 3a, b which shows TEM image of $PMMA_{10K}$@$PHEMA_{5K}$ micelles compared with those crosslinked with DETA. $PMMA_{10K}$@$PHEMA_{5K}$ micelles without DETA had spherical shapes with a particle diameter approximately 500 nm and a broad distribution of the particle size. After an addition of DETA, the micelles became smaller with a diameter approximately 150 nm and more uniform.

TEM images of Ni-loaded PMMA@PHEMA are displayed in Fig. 3c, d. The uniform spherical particles almost in replica to their micellar predecessor were observed indicating that Ni(II) complex was selectively solubilized and subsequently reduced to Ni metal in PMMA@PHEMA micelles. The mean particle diameters obtained from TEM images were 98.5 ± 26.9 and 102.7 ± 23.8 nm for Ni-loaded $PMMA_{10K}$@$PHEMA_{5K}$ and Ni-loaded $PMMA_{12K}$@

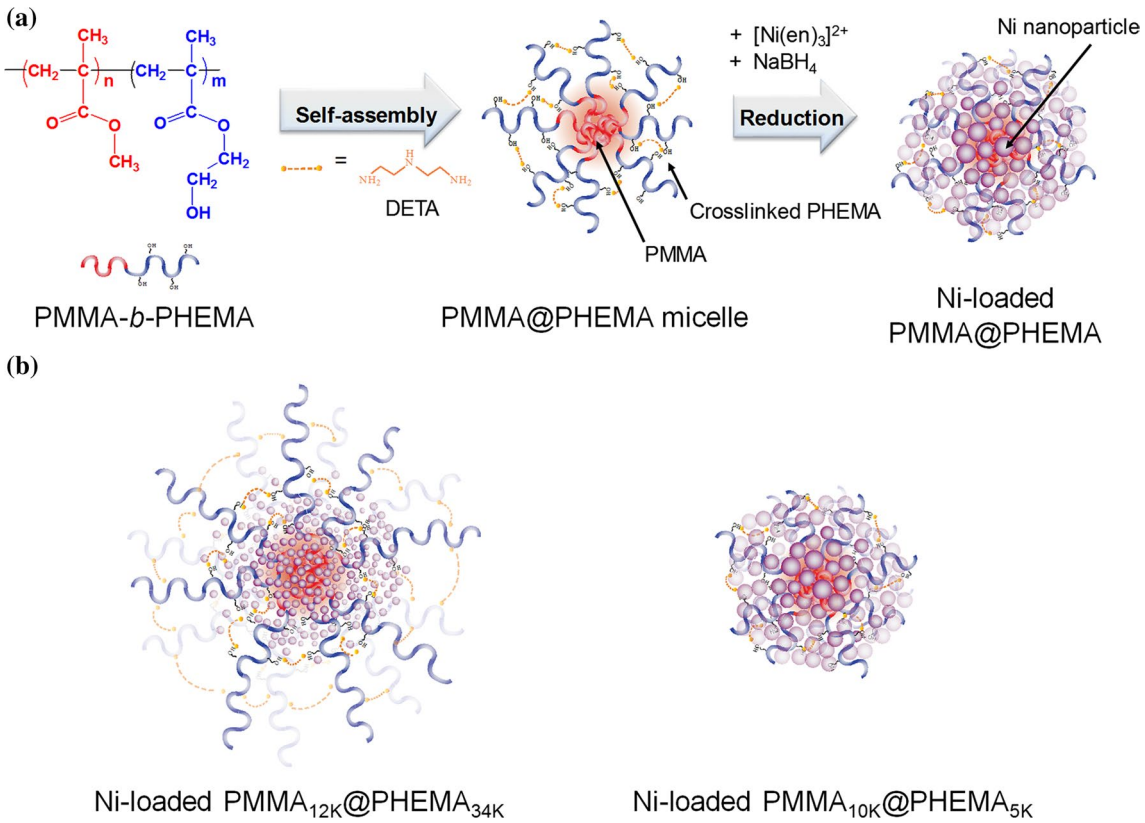

Fig. 2 Schematic pictures of **a** PMMA@PHEMA micelle formation with DETA and subsequent formation of Ni-loaded PMMA@PHEMA and **b** Ni-loaded PMMA@PHEMA

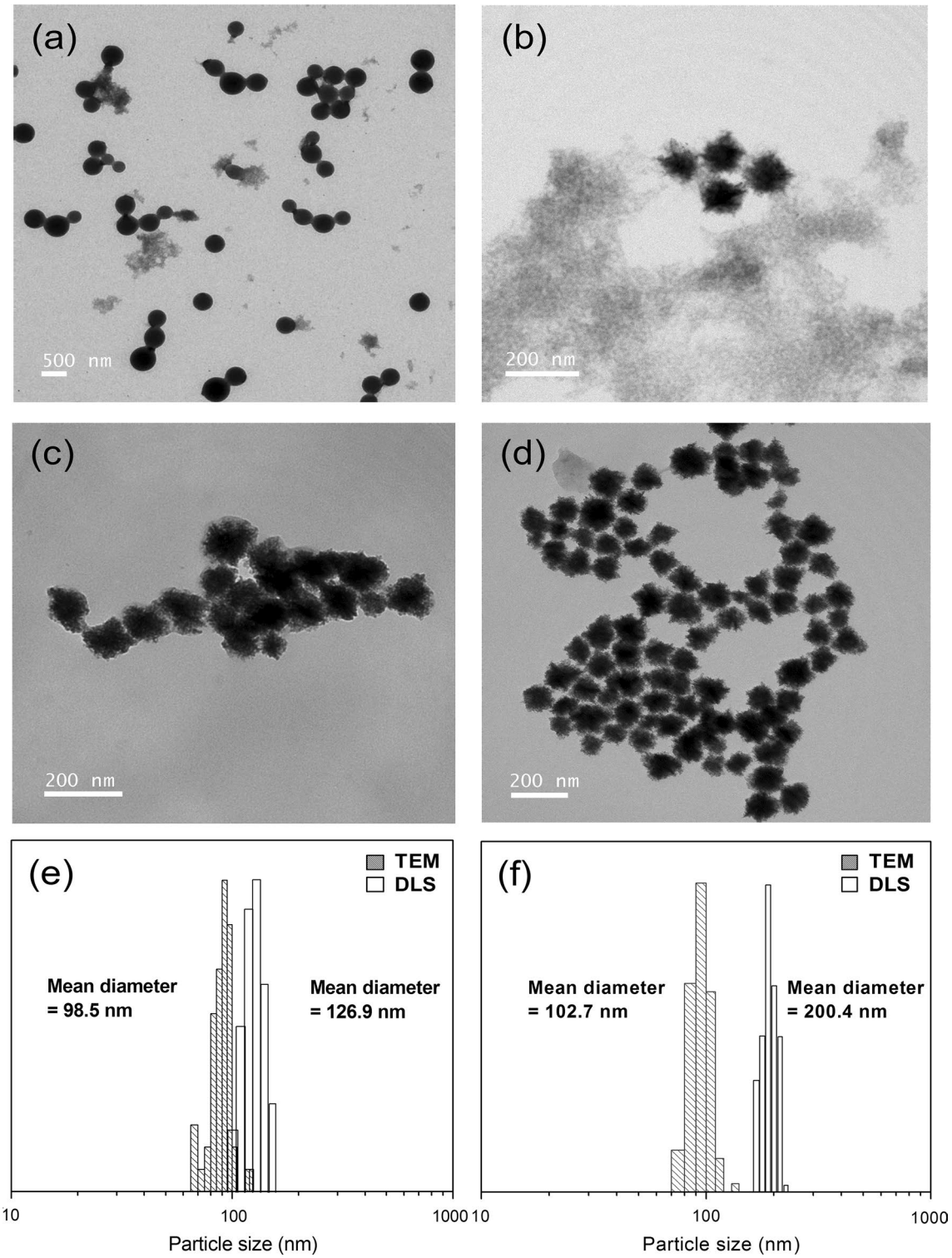

Fig. 3 TEM images of $PMMA_{10K}$@$PHEMA_{5K}$ micelles without DETA **a** and with DETA **b**; TEM images of Ni-loaded $PMMA_{10K}$@$PHEMA_{5K}$ **c** and Ni-loaded $PMMA_{12K}$@$PHEMA_{34K}$ **d**; and a comparison of the particle diameter distributions obtained from TEM and DLS of Ni-loaded $PMMA_{10K}$@$PHEMA_{5K}$ **e** and Ni-loaded $PMMA_{12K}$@$PHEMA_{34K}$ **f**

$PHEMA_{34K}$, respectively. In most cases, the particle sizes of polymeric particles observed through TEM were less than the apparent sizes of polymer particles under dispersion in solvent due to the shrinkage of polymer under a dry state in TEM observation. Therefore, the particle sizes of Ni-loaded PMMA@PHEMA were further determined by dynamic light scattering (DLS) under dispersion in DI water as demonstrated by the particle size distributions shown in Fig. 3e, f. It is evidenced that the mean particle diameters measured by DLS were 126.9 ± 19.1 nm and 200.4 ± 22.8 for nm Ni-loaded $PMMA_{10K}$@$PHEMA_{5K}$ and Ni-loaded $PMMA_{12K}$@$PHEMA_{34K}$, respectively, which were larger than those measured by TEM. This is because PHEMA-shell of Ni-loaded PMMA@PHEMA was expanded under dispersion in water. In addition, narrow particle size distributions of Ni-loaded PMMA@PHEMA indicate that the formation of large aggregates was minimal. Accordingly, PHEMA-shell thicknesses are approximately equal to a half of the diameter differences of the particles in the dispersion and those measured by TEM. Thus, the PHEMA-shell thicknesses were approximately 18 and 52 nm for Ni-loaded $PMMA_{10K}$@$PHEMA_{5K}$ and $PMMA_{12K}$@$PHEMA_{34K}$, respectively.

TEM images of a single Ni-loaded PMMA@PHEMA are demonstrated in Fig. 4a, b which reveal clusters of Ni nanoparticles incorporated within PMMA@PHEMA micelles. However, the sizes of incorporated Ni nanoparticles were significantly different between the particles generated in $PMMA_{10K}$@$PHEMA_{5K}$ micelle and $PMMA_{12K}$@$PHEMA_{34K}$ micelle as shown in the insets of Fig. 4a, b. While the size of Ni nanoparticles in $PMMA_{10K}$@$PHEMA_{5K}$ micelle was approximately 9–15 nm, the size of those incorporated with $PMMA_{12K}$@$PHEMA_{34K}$ micelle was almost an order of magnitude smaller. An existence of nickel metal generated in PMMA@PHEMA micelles was confirmed by HRTEM images shown in Fig. 4c, d. Lattice lines of nickel atoms were fairly observed with the line spacing being 0.175 and 0.205 nm corresponding, respectively, to (200) and (111) Ni lattice planes (Du et al. 2004; Bai et al. 2014). Amounts of Ni incorporated within PMMA@PHEMA micelles were determined

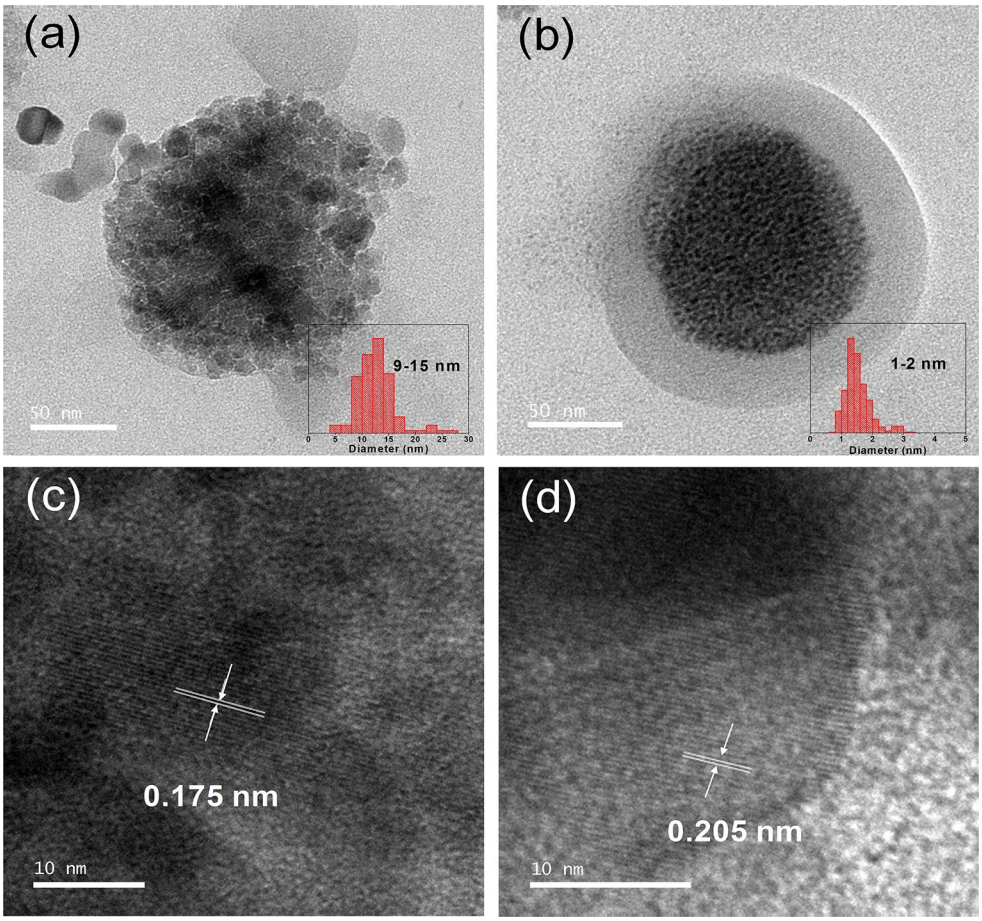

Fig. 4 TEM images of Ni particles in $PMMA_{10K}$@$PHEMA_{5K}$ micelle **a** and $PMMA_{12K}$@$PHEMA_{34K}$ micelle **b**; HRTEM images of Ni in $PMMA_{10K}$@$PHEMA_{5K}$ revealing Ni lattice planes: (200) **c** and (111) **d**; insets of figures a and b are the particle size distributions of Ni particles in $PMMA_{10K}$@$PHEMA_{5K}$ micelle and $PMMA_{12K}$@$PHEMA_{34K}$ micelle, respectively. The samples were not stained by OsO_4

by ICP-OES as summarized in Table S2 in supporting information. Apparently, the amount of Ni incorporated in $PMMA_{12K}$@$PHEMA_{34K}$ was 6 times lower than that in $PMMA_{10K}$@$PHEMA_{5K}$. This suggests that a thicker PHEMA shell of $PMMA_{12K}$@$PHEMA_{34K}$ micelles may impede a transfer of nickel(II)tris(ethylenediamine) complex into the micelles. Although TEM images revealed distinctively a difference in size of Ni particles between both micelles, identifying the primary particles out of the cluster using only TEM images was inaccurate leading to errors in determining the specific surface areas of incorporated Ni nanoparticles on each micelle.

Catalytic reduction of 4-NP by Ni-loaded PMMA@PHEMA

Effect of catalyst concentration

Catalytic activity of Ni-loaded PMMA@PHEMA was evaluated using the reduction of 4-NP to 4-AP in aqueous solution of $NaBH_4$. This reaction has been employed as the model reaction for studying the catalytic performance of metal nanoparticles because the reaction proceeds under mild conditions with large difference of the kinetic rates between the presence and the absence of the catalyst (Aditya et al. 2015). In addition, a progress of the reduction can be conveniently followed by UV–Vis spectrometer through the evolution of UV spectra with time. As shown

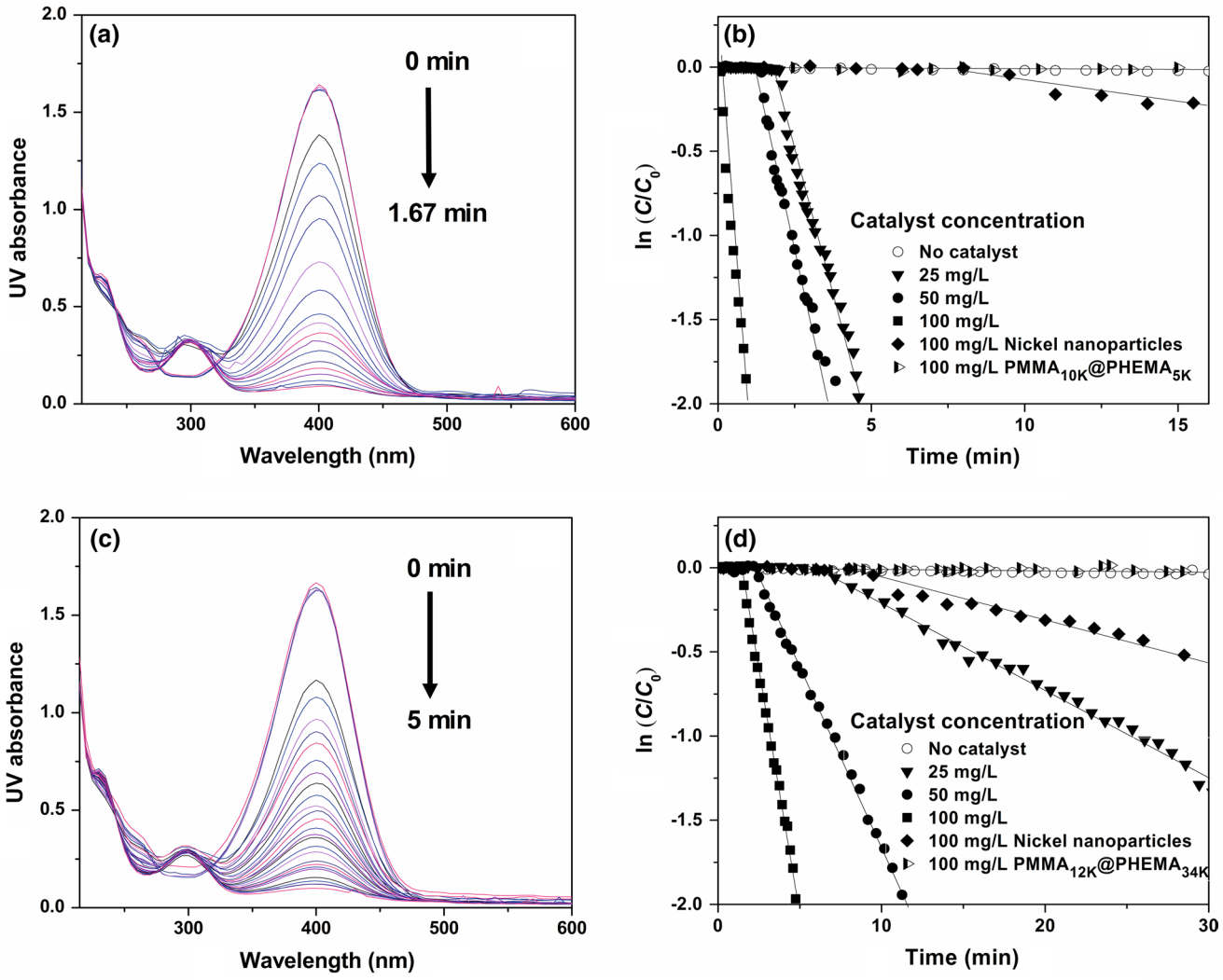

Fig. 5 Evolution of UV absorbance spectra of the catalytic reduction of 4-NP by Ni-loaded $PMMA_{10K}$@$PHEMA_{5K}$ **a** and Ni-loaded $PMMA_{12K}$@$PHEMA_{34K}$ **c**; pseudo-first-order kinetic plots of the catalytic reduction of 4-NP by Ni-loaded $PMMA_{10K}$@$PHEMA_{5K}$ **b** and Ni-loaded $PMMA_{12K}$@$PHEMA_{34K}$ **d** at different catalyst concentrations. The reaction conditions were temperature = 30°C and $[NaBH_4]/[4\text{-NP}] = 50$

in Fig. 5a, c, a disappearance of 4-NP during a progress of the reaction was monitored by the peak intensity at 400 nm which belongs to *p*-nitrophenolate anions, a dissociated form of 4-NP under alkaline conditions. Concomitantly, a production of 4-AP can be followed through a peak evolution at 300 nm. The isosbestic points at 280 and 310 nm indicate that 4-NP was converted only to 4-AP without the side reactions (Wunder et al. 2010).

Amount of $NaBH_4$ was used in excess to that of 4-NP, and typical [$NaBH_4$]/[4-NP] was 50, to ensure that the reaction kinetic followed the pseudo-first-order reaction with respect to 4-NP concentration (C) (Sahiner et al. 2010), i.e.

$$-\frac{dC}{dt} = k_{app}C \tag{1}$$

$$\ln\frac{C}{C_0} = -k_{app}t \tag{2}$$

where k_{app} is the apparent rate constant (min^{-1}) and C_0 is an initial concentration of 4-NP. The kinetic plots of 4-NP reduction catalyzed by Ni-loaded PMMA@PHEMA are presented in Fig. 5b, d. The reduction of 4-NP to 4-AP without Ni-loaded PMMA@PHEMA was almost infeasible but it still followed the pseudo-first-order kinetic with very low $k_{app} = 3.0\times10^{-3}$ min^{-1}. This is because the reduction of 4-NP in the presence of solely $NaBH_4$ is in fact thermodynamically favorable; however, the activation energy of the reaction is very large (Seo et al. 2013). Similarly, the presence of both $PMMA_{10K}$@$PHEMA_{5K}$ and $PMMA_{12K}$@$PHEMA_{34K}$ micelles, without loaded-Ni, did not provide any catalytic effect on the reduction of 4-NP. Upon the addition of Ni-loaded PMMA@PHEMA, the reduction of 4-NP did not start immediately, but after the stagnation period known as the induction time (t_0) (Wunder et al. 2010). It has been explained that the induction time in the reaction catalyzed by metal nanoparticles is the time required for the restructuring of metal surface upon adsorption of the reactant (Wunder et al. 2010; Zhou et al. 2010). This is confirmed in Fig. 6c where the reciprocal induction time ($1/t_0$) increased fairly proportional to an increase in the catalyst concentrations (Wunder et al. 2011). Furthermore for the whole range of catalyst concentration, t_0 of Ni-loaded $PMMA_{12K}$@$PHEMA_{34K}$ were longer compared with those of Ni-loaded $PMMA_{10K}$@$PHEMA_{5K}$ due to its lower nickel content.

After the induction periods, the catalytic reduction of 4-NP by Ni-loaded PMMA@PHEMA was evidenced by a linear descending of $\ln(C/C_0)$ with time as shown in Fig. 5b, d. k_{app} obtained from the slopes of the linear regions were plotted against the catalyst concentration as demonstrated in Fig. 6a. It is apparent that k_{app} of 4-NP reduction increased linearly with the catalyst concentration which is generally observed for the heterogeneous catalysis (Jana et al. 2006; Chen et al. 2008). Due to larger amount of incorporated Ni, Ni-loaded $PMMA_{10K}$@$PHEMA_{5K}$ possessed higher k_{app} and faster ascending of k_{app} as increasing the catalyze concentration compared with that of Ni-loaded $PMMA_{12K}$@$PHEMA_{34K}$. The normalization of k_{app} by amount of incorporated Ni, κ_{nor}, resulted in a merging of two linear lines in Fig. 6a into a single one as revealed in Fig. 6b suggesting a dependence of k_{app} on amount of Ni in PMMA@PHEMA micelles. In fact under the heterogeneous catalytic system, k_{app} is strictly related to the catalytically active surface area (Wunder et al. 2010). However, the determination of accurate catalytic active areas of Ni nanoparticles in PMMA@PHEMA from TEM images was not possible; therefore, the normalization of k_{app} by surface area of Ni nanoparticles did not attempt. The role of PMMA@PHEMA micelles in enhancing the catalytic activity of Ni is also highlighted in Fig. 5b, d. As comparing the kinetic plots of Ni-loaded $PMMA_{10K}$@$PHEMA_{5K}$ and Ni-loaded $PMMA_{12K}$@$PHEMA_{34K}$ to that of bare Ni nanoparticles under the catalyse concentration of 100 mg/L, it is obvious that t_0 as well as k_{app} were significantly improved for Ni nanoparticles in the presence of PMMA@PHEMA micelles.

Mechanistically, the catalytic reduction of 4-NP by metal nanoparticles undergoes primarily on the surface of metal nanoparticles; therefore, both BH_4^- and 4-NP (nitrophenolate anions) must reach the surface of Ni nanoparticles prior to the reduction to occur (Veerakumar et al. 2012). This leads to the argument that under the present condition in which Ni nanoparticles were encapsulated in PMMA@PHEMA micelles, the diffusion to Ni particle surfaces may be the rate-determining step. To justify that, the theoretical bimolecular rate constant (k_{bm}) was employed as expressed in Eq. (3) (Graetzel and Frank 1982).

$$\frac{1}{k_{bm}} = \frac{1}{4\pi r^2}\left(\frac{1}{k_{et}} + \frac{r}{D}\right) \tag{3}$$

where r is the radius of particle (a micelle), k_{et} is the rate of electron transport and D is the diffusion coefficient of the reactant. For the diffusion-controlled reaction, k_{et} is much larger than D; therefore, Eq. (3) is reduced to the Smoluchowski equation

$$k_{bm} = 4\pi rD \tag{4}$$

Taking the diffusion coefficient of 4-NP equal to 6.92×10^{-6} cm^2/s (Johnson et al. 2013), the theoretical k_{bm} was estimated to be 5.02×10^{-10} $cm^3/s{\cdot}$particle for Ni-loaded $PMMA_{10K}$@$PHEMA_{5K}$ and 8.71×10^{-10} $cm^3/s{\cdot}$particle for Ni-loaded $PMMA_{12K}$@$PHEMA_{34K}$. The experimental k_{bm} was determined from the slopes of the plots in Fig. 6a. They equal to 8.05×10^{-13} $cm^3/s{\cdot}$particle for Ni-loaded $PMMA_{10K}$@$PHEMA_{5K}$ and 6.05×10^{-13} $cm^3/s{\cdot}$particle for

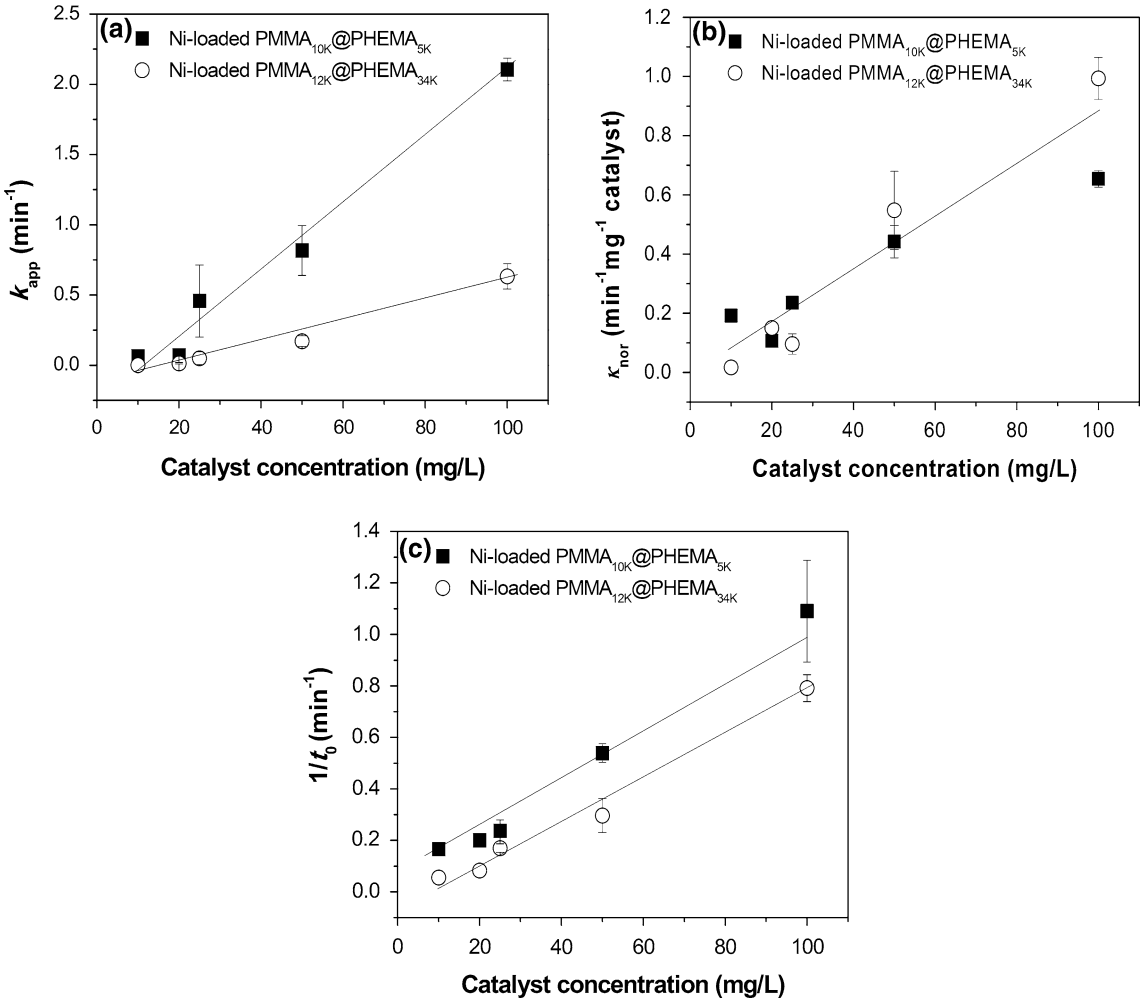

Fig. 6 Effect of catalyst concentration on k_{app} **a**, κ_{nor} **b** and $1/t_0$ **c** for the catalytic reduction of 4-NP by Ni-loaded PMMA@PHEMA

Ni-loaded $PMMA_{12K}$@$PHEMA_{34K}$. Evidently, theoretical k_{bm}s were approximately three orders of magnitude larger than experimental k_{bm}s. Therefore, the catalytic reduction of 4-NP by Ni-loaded PMMA@PHEMA was not limited by the diffusion process (Johnson et al. 2013).

Effect of DETA shell crosslinker

Ni-loaded $PMMA_{12K}$@$PHEMA_{34K}$ was prepared under different [DETA]/[$PMMA_{12K}$@$PHEMA_{34K}$] ratios to investigate the effect of DETA on the catalytic activity as presented in Fig. 7. It is clear from the kinetic plots that the reduction rate of 4-NP increased as increasing of [DETA]/[$PMMA_{12K}$@$PHEMA_{34K}$] ratio. Accordingly, the k_{app} and t_0 of the 4-NP reduction in the presence of Ni-loaded $PMMA_{12K}$@$PHEMA_{34K}$ prepared with different [DETA]/[$PMMA_{12K}$@$PHEMA_{34K}$] ratios are summarized in Table 2.

Increase in DETA amount improved markedly the catalytic activity of Ni-loaded $PMMA_{12K}$@$PHEMA_{34K}$,

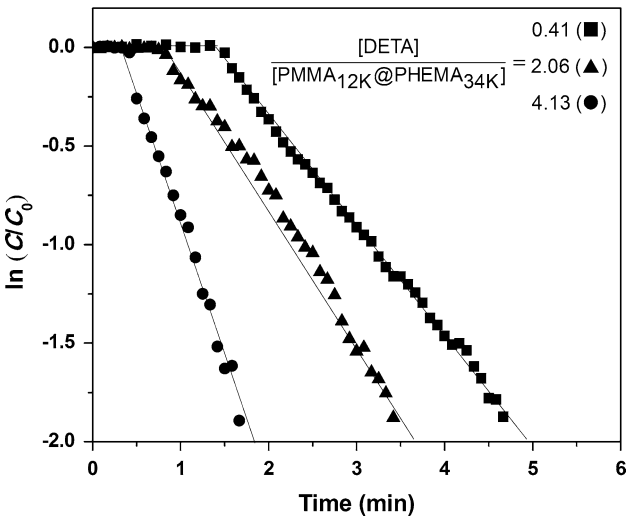

Fig. 7 Pseudo-first-order kinetic plots of the catalytic reduction of 4-NP by Ni-loaded $PMMA_{12K}$@$PHEMA_{34K}$ prepared with different [DETA]/[$PMMA_{12K}$@$PHEMA_{34K}$] ratios

Table 2 k_{app} and t_0 of the catalytic reduction of 4-NP by Ni-loaded $PMMA_{12K}$@$PHEMA_{34K}$ prepared with different [DETA]/[$PMMA_{12K}$@$PHEMA_{34K}$] ratios

$\frac{[DETA]}{[PMMA_{12K}@PHEMA_{34K}]}$	k_{app} (min^{-1})	t_0 (min)	R^2
0.41	0.61	1.66	0.99
2.06	0.78	1.00	0.98
4.13	1.73	0.41	0.96

as indicated by a reduction of t_0 and an increase of k_{app}. DETA was added during the formation of $PMMA_{12K}$@$PHEMA_{34K}$ micelles prior to the generation of Ni nanopartices which resulted in a decrease in the amount of incorporated Ni with increasing DETA concentration (see Table S2 in supporting information). This indicates that an improvement of the catalytic activity is primarily due to increasing amount of DETA not the amount of incorporated Ni. Such improvement in Ni-loaded $PMMA_{12K}$@$PHEMA_{34K}$ upon an increase in [DETA]/[$PMMA_{12K}$@$PHEMA_{34K}$] ratio is a consequence of an enhancement of BH_4^- and 4-NP adsorptions on the micelle generated by the specific interactions between both reactants and amine functional group of DETA. This enhanced catalytic activity has also been observed in metal nanoparticles stabilized by polymers bearing amine functional groups (You et al. 2017; Verma et al. 2015) which impart strong attractions toward BH_4^- and 4-NP. Nevertheless, the present study has revealed experimentally that the catalytic reduction of 4-NP in polymer-stabilized metal nanoparticles can be alternatively improved by an incorporation of the amine-containing crosslinker and its content.

Furthermore, the effect of DETA is evidenced in the reusability test of Ni-loaded PMMA@PHEMA as presented in Fig. 8. The reusability was performed by reducing 4-NP for five times consecutively in the presence of the catalysts. Apparently, the reduction of 4-NP to 4-AP reached a full conversion on every cycles of the reduction; however, the catalytic rates showed progressive decline after the first cycle. The decline of the reduction rate is due to a binding of 4-AP, the reaction product, on the catalytic-active sites (Zhou et al. 2010). As shown in Fig. 8a, Ni-loaded $PMMA_{10K}$@$PHEMA_{5K}$ possessed a better reusability as compared with those of Ni-loaded $PMMA_{12K}$@$PHEMA_{34K}$ because of the higher content of Ni. In comparison among Ni-loaded $PMMA_{12K}$@$PHEMA_{34K}$ prepared with different [DETA]/[$PMMA_{12K}$@$PHEMA_{34K}$] ratios, despite low incorporated Ni in higher [DETA]/[$PMMA_{12K}$@$PHEMA_{34K}$] ratio, the reusability was improved with increased amount of DETA as suggested by a shorter reaction time to reach a full conversion of 4-NP and higher k_{app} on each reduction cycle.

Comparison of catalytic performance of Ni-loaded PMMA@PHEMA with that of other Ni-containing catalysts

Catalytic performances of Ni-loaded PMMA@PHEMA and those of other Ni-containing catalysts reported in the literatures are presented in the plot of κ_{nor} (min^{-1} mg^{-1} Ni) against mg of Ni as shown in Fig. 9. Such a plot allows a prompt comparison of the catalytic performance under different catalyst concentrations. A high-performance catalyst occupies the region on a top left corner of the plot indicating a high catalytic rate constant at minimal usage of the catalyst. Evidently, both Ni-loaded $PMMA_{10K}$@$PHEMA_{5K}$ and Ni-loaded $PMMA_{12K}$@$PHEMA_{34K}$ possessed excellent catalytic performances compared with those of previous studies.

Conclusions

Ni nanoparticles were generated in PMMA@PHEMA core-crosslinked-shell micelles prepared from PMMA-*b*-PHEMA copolymers with different molecular weight of each segment, namely Ni-loaded $PMMA_{10K}$@$PHEMA_{5K}$ and Ni-loaded $PMMA_{12K}$@$PHEMA_{34K}$. The particle size of Ni nanoparticles formed in $PMMA_{10K}$@$PHEMA_{5K}$ micelle was 9 to 15 nm which was almost an order of magnitude larger than the size of Ni nanoparticles in $PMMA_{12K}$@$PHEMA_{34K}$ micelle. HRTEM revealed an existence of Ni atoms in PMMA@PHEMA micelles with Ni line spacing being 0.175 and 0.205 nm corresponding, respectively, to (200) and (111) lattice planes. Ni-loaded PMMA@PHEMA was employed as the catalyst for the reduction of 4-NP to 4-AP in aqueous solution under ambient condition. k_{app} of Ni-loaded $PMMA_{10K}$@$PHEMA_{5K}$ was higher with steeper ascending of k_{app} with increasing the catalyst concentration compared with those observed in Ni-loaded $PMMA_{12K}$@$PHEMA_{34K}$. This is because of the larger amount of Ni content in $PMMA_{10K}$@$PHEMA_{5K}$. In addition, k_{app} is dependent on the micelle structure and the amount of PHEMA-shell crosslinker. The catalytic

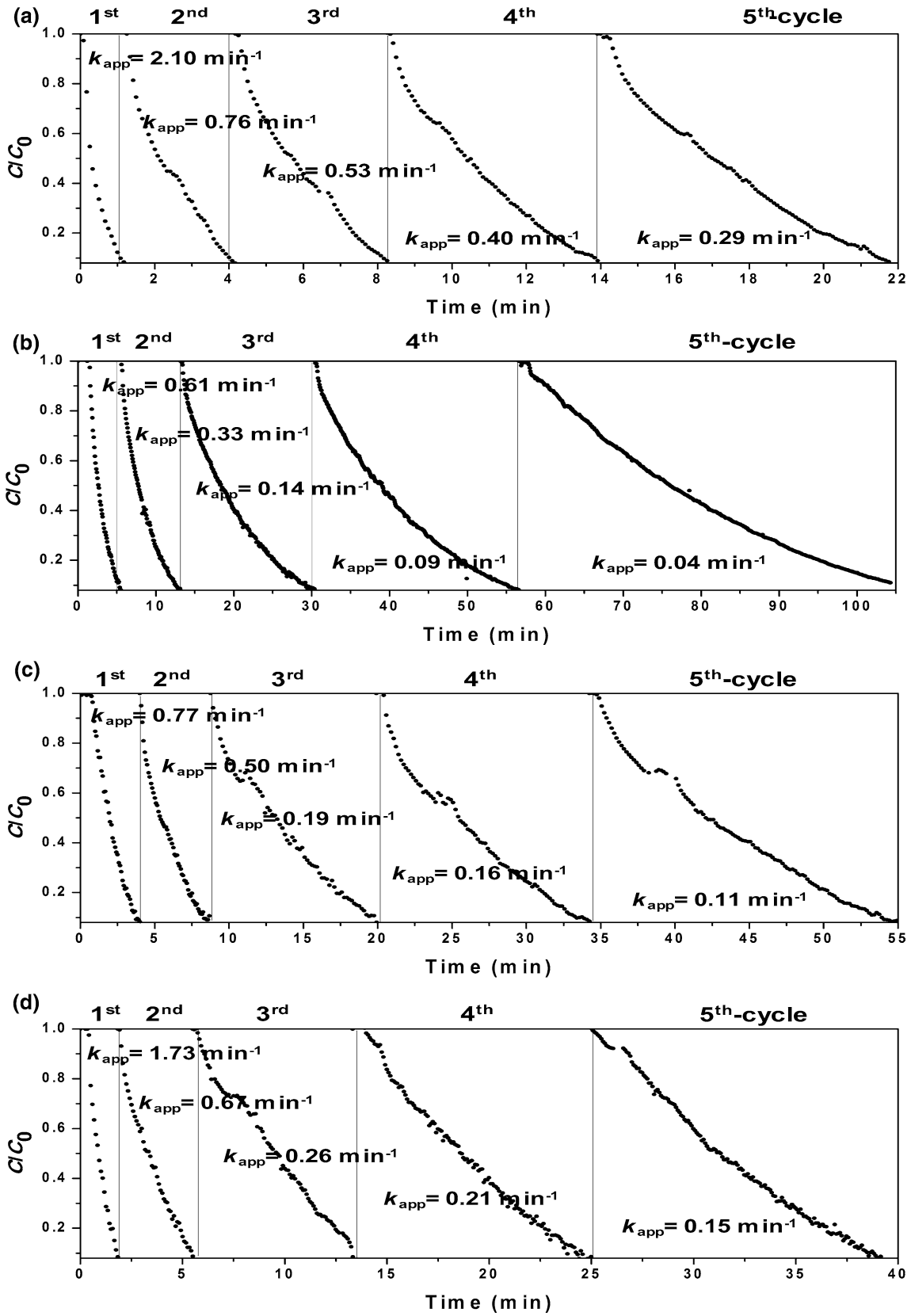

Fig. 8 Effect of DETA on the reusability of Ni-loaded PMMA@PHEMA: **a** [DETA]/[$PMMA_{10K}$@$PHEMA_{5K}$] = 0.41, **b** [DETA]/[$PMMA_{12K}$@$PHEMA_{34K}$] = 0.41, **c** [DETA]/[$PMMA_{12K}$@$PHEMA_{34K}$] = 2.06 and **d** [DETA]/[$PMMA_{12K}$@$PHEMA_{34K}$] = 4.13. The reaction conditions were temperature = 30°C and [$NaBH_4$]/[4-NP] = 50

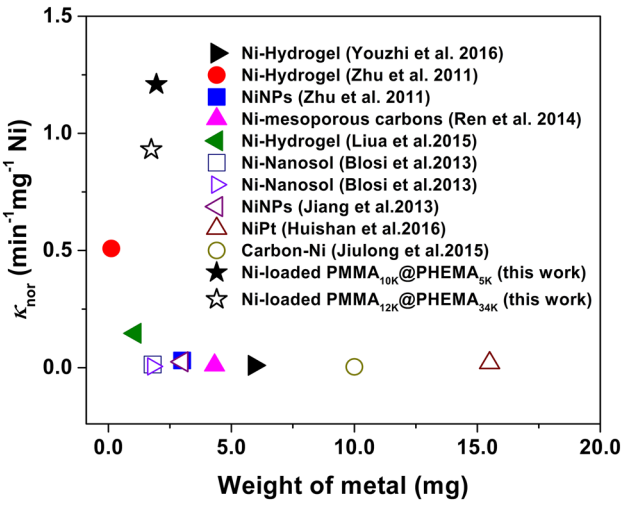

Fig. 9 Plot of the normalized rate constant (κ_{nor}) versus amount of metal for a comparison of the catalytic performance in the reduction of 4-NP

performance of Ni-loaded $PMMA_{12K}$@$PHEMA_{34K}$ was markedly improved upon increase in the amount of PHEMA-shell crosslinker.

Acknowledgements This project is supported by Thailand Research Fund (TRF), Synchrotron Light Research Institute (SLRI) and Khon Kaen University (KKU) under TRF research scholar program (Grant no. RSA5980075). The partial supports from PERCH-CIC and National Research University Project of Thailand, Office of the Higher Education Commission through Biofuel Cluster of Khon Kaen University are acknowledged (Grant No. NRU57).

Compliance with ethical standards

Conflict of interest On behalf of all authors, the corresponding author states that there is no conflict of interest.

References

Aditya T, Pal A, Pal T (2015) Nitroarene reduction: a trusted model reaction to test nanoparticle catalysts. Chem Commun 51:9410–9431

Alexandridis P, Tsianou M (2011) Block copolymer-directed metal nanoparticle morphogenesis and organization. Eur Polym J 47:569–583

Ananikov VP (2015) Nickel: the "spirited horse" of transition metal catalysis. ACS Catal 5:1964–1971

Antonietti M, Förster S, Hartmann J, Oestreich S (1996) Novel amphiphilic block copolymers by polymer reactions and their use for solubilization of metal salts and metal colloids. Macromolecules 29:3800–3806

Astafieva I, Khougaz K, Eisenberg A (1995) Micellization in block polyelectrolyte solutions. 2. fluorescence study of the critical micelle concentration as a function of soluble block length and salt concentration. Macromolecules 28:7127–7134

Astruc D (2008) Nanoparticles and catalysis. Wiley-VCH GmbH & Co. KGaA, Weinheim

Bai L, Lirui L, Zhenyu Z (2014) Molecular dynamics simulation for arrangement of nickel atoms filled in carbon nanotubes. J Appl Phys 116:084305. https://doi.org/10.1063/1.4893023

Baruah B, Gabriel GJ, Akbashev MJ, Booher ME (2013) Facile Synthesis of silver nanoparticles stabilized by cationic polynorbornenes and their catalytic activity in 4-nitrophenol reduction. Langmuir 29:4225–4234

Blosi M, Albonetti S, Costa AL, Sangiorgi N, Sanson A (2013) Easily scalable synthesis of Ni nanosols suitable for the hydrogenation of 4-nitrophenol to 4-aminophenol under mild condition. Chem Eng J 215–216:616–625

Chen X, Zhao D, An Y, Zhang Y, Cheng J, Wang B, Shi L (2008) Formation and catalytic activity of spherical composites with surfaces coated with gold nanoparticles. J Colloid Interface Sci 322:414–420

Cuenya BR (2013) Metal nanoparticle catalysts beginning to shape-up. Acc Chem Res 46:1682–1691

Demirci S, Sahiner N (2015) The use of metal nanoparticle-embedded poly(ethyleneimine) composite microgel in the reduction of nitrophenols. Water Air Soil Pollut 226:64

Dionigi C, Lungaro L, Goranov V, Riminucci A, Piñeiro-Redondo V, Bañobre-López M, Rivas J, Dediu V (2014) Smart magnetic poly(*N*-isopropylacrylamide) to control the release of bio-active molecules. J Mater Sci Mater Med 25:2365–2371

Du Y, Chen H, Chen R, Xu N (2004) Synthesis of *p*-aminophenol from *p*-nitrophenol over nano-sized nickel catalysts. Appl Catal A 277:259–264

Fan Q, Li X, Yang Z, Han J, Xu S, Zhang F (2016) Double-confined nickel nanocatalyst derived from layered double hydroxide precursor: atomic scale insight into microstructure evolution. Chem Mater 28:6296–6304

Farooqi ZH, Iqbal S, Khan SR, Kanwal F, Begum R (2014) Cobalt and nickel nanoparticles fabricated poly(n-isopropylacrylamide-*co*-acrylic acid) microgels for catalytic applications. e-Polymers 14:313–321

Gangula A, Podila R, Karanam RML, Janardhana C, Rao AM (2011) Catalytic reduction of 4-nitrophenol using biogenic gold and silver nanoparticles derived from Breynia rhamnoides. Langmuir 27:15268–15274

Graetzel M, Frank AJ (1982) Interfacial electron-transfer reactions in colloidal semiconductor dispersions, kinetic analysis. J Phys Chem 86:2964–2967

Huishan S, Kecheng P, Lu Z, Bing Z, Xu X (2016) Enhanced activity of supported Ni catalysts promoted by Pt for rapid reduction of aromatic nitro compounds. Nanomaterials 6:103. https://doi.org/10.3390/nano6060103

Jana S, Ghosh SK, Nath S, Pande S, Praharaj S, Panigrahi S, Basu S, Endo T, Pal T (2006) Synthesis of silver nanoshell-coated cationic polystyrene beads: a solid phase catalyst for the reduction of 4-nitrophenol. Appl Catal A 313:41–48

Jiang Z, Xie J, Jiang D, Wei X, Chena M (2013) Modifiers-assisted formation of nickel nanoparticles and their catalytic application to *p*-nitrophenol reduction. Cryst Eng Commun 15:560–569

Jiang C, Shang Z, Liang X (2015) Chemoselective transfer hydrogenation of nitroarenes catalyzed by highly dispersed, supported nickel nanoparticles. ACS Catal 5:4814–4818

Jiulong L, Jeong WK, Weon BK (2015) Kinetics and catalytic activity of carbon-nickel nanocomposites in the reduction of 4-nitrophenol. Elastomers Compos 50:217–222

Johnson JA, Makis JJ, Marvin KA, Rodenbusch SE, Stevenson KJ (2013) Size-dependent hydrogenation of *p*-nitrophenol with Pd nanoparticles synthesized with poly(amido)amine dendrimer templates. J Phys Chem C 117:22644–22651

Kang N, Perron M-È, Prud'homme RE, Zhang Y, Gaucher G, Leroux J-C (2005) Stereocomplex block copolymer micelles: core–shell nanostructures with enhanced stability. Nano Lett 5:315–319

Karakas K, Celebioglu A, Celebi M, Uyar T, Zahmakiran M (2017) Nickel nanoparticles decorated on electrospun polycaprolactone/chitosan nanofibers as flexible, highly active and reusable nanocatalyst in the reduction of nitrophenols under mild conditions. Appl Catal B 203:549–562

Liua J, Wanga J, Wanga Y, Liua C, Jina M, Xua Y, Lia L, Guoa X, Hub A, Liuc T, Lincolnd SF, Prud'hommee RK (2015) A thermosensitive hydrogel carrier for nickel nanoparticles. Colloids Interface Sci Commun 4:1–4

Mortensen PM, Grunwaldt J-D, Jensen PA, Jensen AD (2016) Influence on nickel particle size on the hydrodeoxygenation of phenol over Ni/SiO_2. Catal Today 259:277–284

Nicolai T, Colombani O, Chassenieux C (2010) Dynamic polymeric micelles versus frozen nanoparticles formed by block copolymers. Soft Matter 6:3111–3118

Panwar V, Kumar A, Singh R, Gupta P, Ray SS, Jain SL (2015) Nickel-decorated graphene oxide/polyaniline hybrid: a robust and highly efficient heterogeneous catalyst for hydrogenation of terminal alkynes. Ind Eng Chem Res 54:11493–11499

Priority Pollutant List (2014) U.S. Environmental Protection Agency

Ren Y, Sun C, Hao S (2014) Facile route fabrication of nickel based mesoporous carbons with high catalytic performance towards 4-nitrophenol reduction. Green Chem 16:2273–2280

Rodríguez-Hernández J, Chécot F, Gnanou Y, Lecommandoux S (2005) Toward 'smart' nano-objects by self-assembly of block copolymers in solution. Prog Polym Sci 30:691–724

Sahiner N, Ozay H, Ozay O, Aktas N (2010) New catalytic route: hydrogels as templates and reactors for in situ Ni nanoparticle synthesis and usage in the reduction of 2- and 4-nitrophenols. Appl Catal A 385:201–207

Seo E, Kim J, Hong Y, Kim YS, Lee D, Kim B-S (2013) Double hydrophilic block copolymer templated Au nanoparticles with enhanced catalytic activity toward nitroarene reduction. J Phys Chem C 117:11686–11693

Tang M, Huang G, Zhang S, Liu Y, Li X, Wang X, Pang X, Qiu H (2014) Low-cost removal of organic pollutants with nickel nanoparticle loaded ordered macroporous hydrogel as high performance catalyst. Mater Chem Phys 145:418–424

Veerakumar P, Velayudham M, Lu K-L, Rajagopal S (2012) Polyelectrolyte encapsulated gold nanoparticles as efficient active catalyst for reduction of nitro compounds by kinetic method. Appl Catal A 439–440:197–205

Verma AD, Mandal RK, Sinha I (2015) Kinetics of *p*-Nitrophenol reduction catalyzed by PVP stabilized copper nanoparticles. Catal Lett 145:1885–1892

Vijayakrishna K, Prabhu Charan KT, Manojkumar K, Venkatesh S, Pothanagandhi N, Sivaramakrishna A, Mayuri P, Senthil Kumar A, Sreedhar B (2016) Ni nanoparticles stabilized by poly(Ionic Liquids) as chemoselective and magnetically recoverable catalysts for transfer hydrogenation reactions of carbonyl compounds. ChemCatChem 8:1139–1145

Wunder S, Polzer F, Lu Y, Mei Y, Ballauff M (2010) Kinetic analysis of catalytic reduction of 4-nitrophenol by metallic nanoparticles immobilized in spherical polyelectrolyte brushes. J Phys Chem C 114:8814–8820

Wunder S, Lu Y, Albrecht M, Ballauff M (2011) Catalytic activity of faceted gold nanoparticles studied by a model reaction: evidence fors-Induced surface restructuring. ACS Catal 1:908–916

Xia J, Di J, Li H, Xu H, Li H, Guo S (2016) Ionic liquid-induced strategy for carbon quantum dots/BiOX (X = Br, Cl) hybrid nanosheets with superior visible light-driven photocatalysis. Appl Catal B 181:260–269

Xu D, Diao P, Jin T, Wu Q, Liu X, Guo X, Gong H, Li F, Xiang M, Ronghai Y (2015) Iridium oxide nanoparticles and iridium/iridium oxide nanocomposites: photochemical fabrication and application in catalytic reduction of 4-nitrophenol. ACS Appl Mater Interfaces 7:16738–16749

You J-G, Shanmugam C, Liu Y-W, Yu C-J, Tseng W-L (2017) Boosting catalytic activity of metal nanoparticles for 4-nitrophenol reduction: modification of metal naoparticles with poly(diallyldimethylammonium chloride). J Hazard Mater 324:420–427

Youzhi G, Yang H, Yiping Z, Li C, Fanyong Y (2016) Fabrication of thermosensitive hydrogel-supported Ni nanoparticles with tunable catalytic activity for 4-nitrophenol. J Mater Sci 51:3200–3210

Zahmakıran M, Özkar S (2011) Metal nanoparticles in liquid phase catalysis; from recent advances to future goals. Nanoscale 3:3462–3481

Zhang Z, Wu Y (2010) Investigation of the $NaBH_4$-induced aggregation of Au nanoparticles. Langmuir 26:9214–9223

Zhao B, Mele G, Pio I, Li J, Palmisano L, Vasapollo G (2010) Degradation of 4-nitrophenol (4-NP) using $Fe–TiO_2$ as a heterogeneous photo-fenton. J Hazard Mater 176:569–574

Zhou X, Xu W, Liu G, Panda D, Chen P (2010) Size-dependent catalytic activity and dynamics of gold nanoparticles at the single-molecule kevel. J Am Chem Soc 132:138–146

Zhu Z, Guo X, Wu S, Zhang R, Wang J, Li L (2011) Preparation of nickel nanoparticles in spherical polyelectrolyte brush nanoreactor and their catalytic activity. Ind Eng Chem 50:13848–13853